Eur Biophys J (1990) 18:317–326

European Biophysics Journal

Open-channel block of Na^+ channels by intracellular Mg^{2+}

M. Pusch *

Max-Planck-Institut für biophysikalische Chemie, Am Fassberg, D-3400 Göttingen, Federal Republic of Germany

Received March 14, 1990/Accepted in revised form May 23, 1990

Abstract. *1.* Macroscopic and single-channel currents through several types of cloned rat brain Na^+ channels, expressed in *Xenopus* oocytes, were measured using the patch-clamp technique. *2.* For all cloned channel types and for endogenous Na^+ channels in chromaffin cells, intracellular Mg^{2+} blocks outward currents in a voltage-dependent manner similar to that in rat brain type II Na^+ channel (Pusch et al. 1989). *3.* A sodium-channel mutant ('cZ-2') with long single-channel open times was used to examine the voltage-dependent reduction of single-channel outward current amplitudes by intracellular Mg^{2+}. This reduction could be described by a simple blocking mechanism with half-maximal blockage at 0 mV in 1.8 m*M* intracellular Mg^{2+} and a voltage-dependence of e-fold per 39 mV (in $\approx$125 m*M* $[Na]_i$); this corresponds to a binding-site at an electrical distance of 0.32 from the inside of the membrane. *4.* At low Mg^{2+} concentrations and high voltages, the open-channel current variance is significantly elevated with respect to zero $[Mg]_i$. This indicates that Mg^{2+} acts as a fast blocker rather than gradually decreasing current, e.g. by screening of surface charges. Analysis of the open-channel variance yielded estimates of the block and unblock rate constants, which are of the order of $2 \cdot 10^8\ M^{-1}\ s^{-1}$ and $3.6 \cdot 10^5\ s^{-1}$ at 0 mV for the mutant cZ-2. *5.* A quantitative analysis of tail-currents of wild-type II channels showed that the apparent affinity for intracellular Mg^{2+} strongly depends on $[Na]_i$. This effect could be explained in terms of a multi-ion pore model. *6.* Simulated action potentials, calculated on the basis of the Hodgkin-Huxley theory, are significantly reduced in their amplitude and delayed in their onset by postulating Mg^{2+} block at physiological levels of $[Mg]_i$.

Key words: Sodium channel – Mg^{2+} block – Open-channel noise – Patch clamp

Introduction

Recent studies have shown that intracellular Mg^{2+} in the millimolar range blocks outward currents through rat brain type II sodium channels in a voltage-dependent manner (Pusch et al. 1989). This Mg^{2+} block could be responsible for the decrease in maximum conductance at high voltages which has been observed in several preparations (Pappone 1980; Almers et al. 1984; Stühmer et al. 1987; Fahlke and Ruppersberg 1988).

The present paper extends the studies of Pusch et al. (1989). Mg^{2+} block occurs in several cloned channel types expressed in *Xenopus* oocytes and, in addition, in 'natural' Na^+ channels of chromaffin cells. Experiments on the mutant Na^+ channel 'cZ-2', which is obtained by 'cutting' the mRNA between homologous repeats III and IV, clarify the mechanism of the block by Mg^{2+}. CZ-2 shows very slow and incomplete inactivation (Stühmer et al. 1989). At the single-channel level the mutant is characterized by a greatly increased mean open time ($\approx$6 ms) with effectively unaltered single-channel conductance ($\approx$13 pS in cell-attached patches with normal frog Ringer in the recording pipette). These long open times allowed to show that the main effect of intracellular Mg^{2+} is a voltage-dependent reduction of the single-channel current amplitude and an increase of the open-channel noise, indicating a fast, flickery block.

The dependence of the Mg^{2+} block on $[Na]_i$ was also investigated. A quantitative analysis of macroscopic tail currents through wild-type II channels shows that the apparent affinity for Mg^{2+} strongly depends on $[Na]_i$. This effect is discussed in terms of a multi-ion pore model.

Apart from its biophysical significance in terms of permeation mechanisms, the Mg^{2+} block may have a physiological significance. Intracellular free Mg^{2+} is strongly coupled to the energy balance of cells via Mg^{2+}-ATP – ADP hydrolysis. Thus high energy consumption

Abbreviations: $[Na]_i$, intracellular Na^+ concentration; $[K]_i$, intracellular K^+ concentration; $[Mg]_i$, intracellular Mg^{2+} concentration; HEPES, N-2-hydroxylethyl piperazine-N-2-ethanesulfonic acid; EGTA, ethyleneglycol-bis-[β-amino-ethyl ether] N,N'-tetra acetic acid; TEA, tetraethylammonium

Present address and address for offprint requests: Istituto di Cibernetica e Biofisica, CNR, Via Dodecaneso 33, I-16146 Genova, Italy

may lead to an increase in free intracellular Mg^{2+} which, apart from its known effects on other channels, significantly modifies action potential firing by decreasing Na^+ conductance. Theoretical calculations of action potentials taking into account Mg^{2+} block are presented. At $[Mg]_i > 0$, action potentials are reduced in their amplitude and delayed in their onset.

The ability to express cloned channels in oocytes makes it possible to compare genetically defined Na^+ channels with respect to their $[Mg]_i$ sensitivity. The comparison of different channel types with respect to their sensitivity to internal Mg^{2+}, concerning open-channel block, and external Ca^{2+}, concerning open-channel block and steady-state activation, will be the subject of the companion paper (Pusch 1990).

Methods

Oocyte injection

Oocytes were injected with mRNA as described by Methfessel et al. (1986). mRNAs for rat brain type II Na^+ channel (Noda et al. 1986), type III Na^+ channel (Kayano et al. 1988) and type II mutants K226Q and cZ-2 (Stühmer et al. 1989) were kindly provided by the group of S. Numa, Kyoto. The preparation of the mutants is described by Stühmer et al. (1989). Briefly, the mutant K226Q is obtained from the wild-type by replacing the lysine at homologous position 226 with glutamine. The mutant cZ-2 is obtained by 'cutting' the cDNA between homologous repeats III and IV. Injection of each single fragment alone does not give rise to measurable Na^+ currents in oocytes; however, injecting an equimolar mixture of both mRNA species results in Na^+ currents with slow and incomplete inactivation (Stühmer et al. 1989).

Current recording

Conventional patch-clamp techniques (Hamill et al. 1981) were used for sodium-current recording. Quasi-macroscopic currents were recorded from large inside-out patches (Pusch et al. 1989) using pipettes pulled from aluminosilicate glass (Hilgenberg) which had resistances between 0.5 and 1.5 MΩ in Ringer. Smaller pipettes pulled from hard borosiliocate glass (Hilgenberg) were used to record single channels from inside-out patches. Current recording and stimulation were controlled by a DEC-PDP-11/73 minicomputer. Macroscopic currents were filtered at 10 kHz with an eight-pole-Bessel filter. Linear leakage and capacitive currents were subtracted on-line using a P/4-method (Bezanilla and Armstrong 1977) for the macroscopic current recordings.

Single-channel recordings were filtered at different frequencies ranging from 3 to 10 kHz. Leakage and capacitive compensation was performed off-line for single-channel recordings using either 'blank' records or scaled leak-pulses to voltages, where no Na^+ channel activation occured, immediately preceding and following application of the main test pulse.

Normal frog Ringer, the primary pipette filling solution (except where indicated), has the following composition (in m*M*): 115 NaCl, 10 NaOH-HEPES, 2.5 KCl, 1.8 $CaCl_2$, pH 7.2. The bath solutions are given in the figure legends. Na^+ currents in chromaffin cells were recorded in the whole-cell configuration of the patch-clamp technique (Marty and Neher 1983). Cells were prepared as described by Fenwick et al. (1982). Solutions for whole-cell recording were (in m*M*): Bath: 140 NaCl, 2.8 KCl, 2 $MgCl_2$, 1 $CaCl_2$, 10 NaOH-HEPES, pH 7.2. Pipette: 120 CsCl, 20 TEACl, 11 NaOH-EGTA, 1 $CaCl_2$, 10 NaOH-HEPES, pH 7.2, and varying amounts of $MgCl_2$.

Analysis

Tail currents were analyzed by fitting an exponential function to the first part of the tail current (excluding the rise time at the beginning of the tail current) and extrapolating this exponential function to the time of the onset of the test pulse. The extrapolated current values were then used to construct instantaneous current-voltage relationships. These reflect the permeability properties of the channel without interference from the kinetic properties since, at the onset of the tail pulse, the degree of activation and inactivation of the channels in the patch is the same.

Single-channel amplitudes were analyzed by threshold analysis; only relatively long and clearly-defined openings were used in compiling histograms.

The open-channel current variance for cZ-2 was analyzed as follows: A variance value was determined for a series of depolarizing steps to the same voltage for one patch. Occasionally flickering of channels was observed even at 0 $[Mg]_i$ (see Fig. 2, lower left trace); only channel openings without obvious flickering were used for the variance analysis. From the selected openings the baseline immediately preceding and following the opening was averaged and subtracted in order to exclude errors due to baseline drifts. These segments of open-channel current were pooled, the variance around the mean was calculated and the variance of analogously-obtained stretches of the baseline was subtracted.

Fitting procedures

All fitting procedures were based on the least-squares criterion, and the simplex algorithm (Caceci and Cacheris 1984) was used for optimization. In order to obtain estimates of the uncertainty of the obtained parameters after fitting, the following procedure was applied: The deviations of the measured values from the optimized model are generally distributed according to a Gaussian function with a standard deviation SD. This standard deviation was used to construct at least 100 synthetic data sets by adding to the original data points pseudo-random numbers which were Gaussian-distributed with a mean of zero and standard deviation SD. The fitting procedure was then applied to these synthetic data sets, yielding, in most cases, a Gaussian distribution for each parameter. The standard deviation of these distributions is a measure

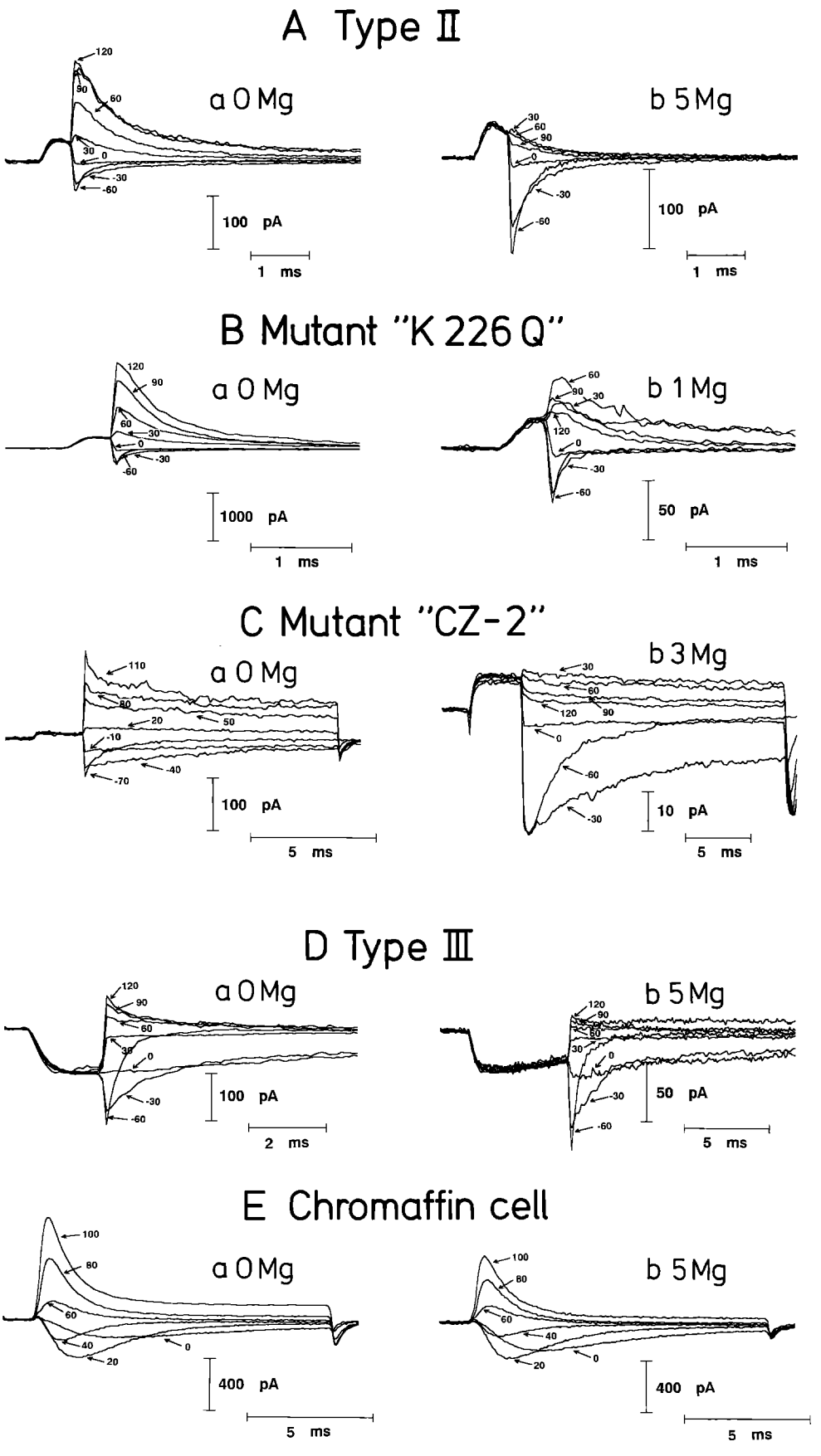

Fig. 1 A–E. Representative current traces at zero (**a**) and at a non-zero (**b**). $[Mg]_i$. The corresponding test voltages are indicated. The Mg^{2+} concentrations are given in m*M*. **A** to **D** shows tail currents measured on inside-out patches from oocytes injected with the corresponding mRNA. The tail-current traces are measured on different inside-out patches; therefore a direct comparison of the overall current magnitude is not possible. The pipette solution in **A** to **D** is normal frog Ringer (see 'Methods'). Apart from the indicated concentration of $MgCl_2$ the bath solution in **A, B** and **C** contained (in m*M*): 105 NaCl, 10 NaOH-HEPES, 10 Na-OH-EGTA, 2.5 KCl, pH 7.2. In **D** 30 NaCl, 90 KCl, 10 KOH-HEPES, 10 KOH-EGTA, pH 7.2. **E** shows whole-cell currents from a chromaffin cell. The currents in **Eb** were obtained from the same cell. The solutions in **E** are given in 'Methods'

of the uncertainty with which this parameter is fixed by the data points.

Temperature

All oocyte experiments were performed at 15 °C. Current recordings from chromaffin cells were done at room temperature (20–24 °C).

Results

1. Effects of intracellular Mg^{2+} on different Na^+ channel types

Intracellular Mg^{2+} blocks Na^+ outward currents in a voltage-dependent manner (Pusch et al. 1989). In order to determine whether this is a general feature of Na^+ channels, the effect of intracellular Mg^{2+} on several Na^+ channel types was tested. Figure 1 shows macroscopic current recordings in the presence and absence of Mg^{2+} for rat brain type II channels (A), for the mutant K226Q (B), for the mutant cZ-2 (C), for the type III channel (D) and for chromaffin cells (E). For those channel types expressed in *Xenopus* oocytes (Fig. 1 A–D) tail currents obtained from inside-out patches are shown. In each case, it is evident that Mg^{2+} reduces the outward currents. An increase in the degree of block with increasing voltage is also apparent. In fact, in records from the cloned channels at high voltages, the Na^+ current decreases despite the increased driving force for Na^+ ions.

The traces in Fig. 1 E have been recorded in the tight-seal whole-cell configuration of the patch-clamp technique (Marty and Neher 1983) from the same chromaffin cell. These cells possess Na^+ channels similar to those of neuronal cells (Fenwick et al. 1982). The currents shown in Fig. 1. E a were recorded with a pipette-solution containing no Mg^{2+}. After the measurement at 0 Mg^{2+}, the pipette was carefully withdrawn; this left the cell intact and allowed a further measurement with a second pipette containing 5 m*M* Mg^{2+} (Fig. 1 Eb). It can be seen that Mg^{2+} also reduces Na^+ outward currents in chromaffin cells although it seems that the effect is less pronounced than in the cloned Na^+ channels. From Fig. 1 E it can also be seen that Mg^{2+} has little effect on gating or the overall magnitude of the current.

2. Block of single-channel outward currents by intracellular Mg^{2+}

Stühmer et al. (1989) have demonstrated that the mutant sodium channel cZ-2 shows very slow and incomplete inactivation after an activating voltage jump from a negative holding voltage. This behavior can be seen in families of tail current traces (Fig. 1 C); here the blocking effect of intracellular Mg^{2+} on macroscopic currents is evident and is similar to that observed in the wild-type II Na^+ channel.

The long open times of cZ-2 channels enabled the Mg^{2+} block to be investigated at the single-channel level.

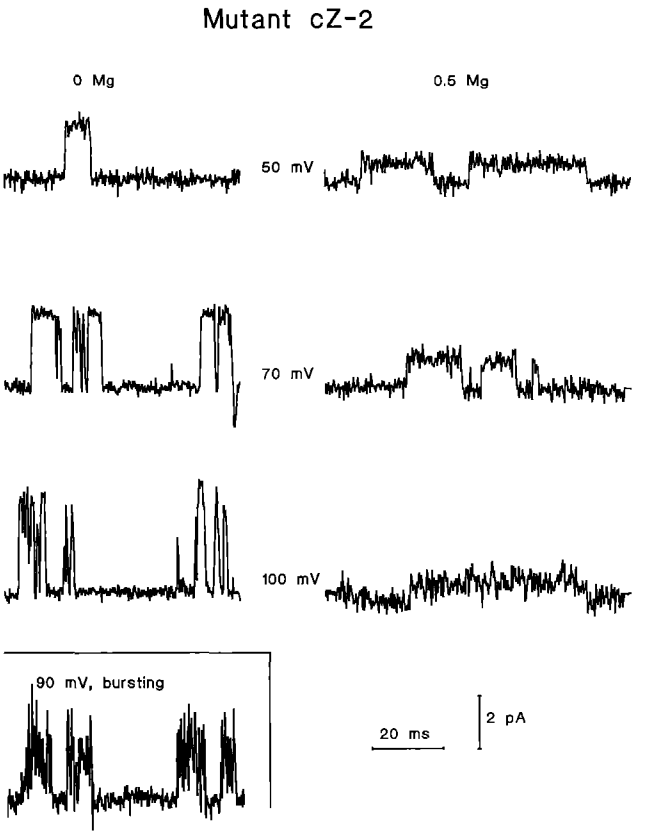

Fig. 2. Single-channel current traces of the mutant cZ-2 from inside-out patches at 0 (left) and 0.5 m*M* (right) $[Mg]_i$. The pipette solution was in all cases normal frog Ringer: the bath solution contained (in m*M*): 105 NaCl, 10 NaOH-HEPES, 10 NaOH-EGTA, 2.5 KCl, pH 7.2. The lower left current trace at 0 Mg^{2+} illustrates the flickery gating sometimes observed independent of the Mg^{2+} concentration used. The current traces were filtered with an 8-pole-Bessel filter with the following cut-off frequencies: 4 kHz (100 mV, 70 mV, 0 Mg^{2+}); 5 kHz (70 mV, 50 mV, 0.5 Mg^{2+}); 10 kHz (50 mV, 90 mV, 0 Mg^{2+}; 100 mV, 0.5 Mg^{2+})

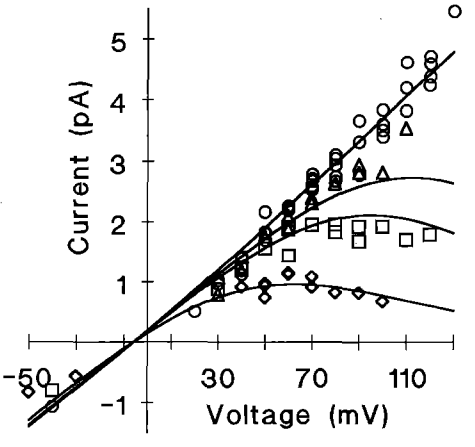

Fig. 3. Single-channel current amplitudes for mutant cZ-2 versus test voltage at different intracellular Mg^{2+} concentrations. Solutions are as in Fig. 2. Circles: 0 $MgCl_2$; Triangles: 0.05 m*M* $MgCl_2$; Squares: 0.1 m*M* $MgCl_2$; Diamonds: 0.5 $MgCl_2$. The solid lines were obtained by a fit of (1) with the parameters given in the text

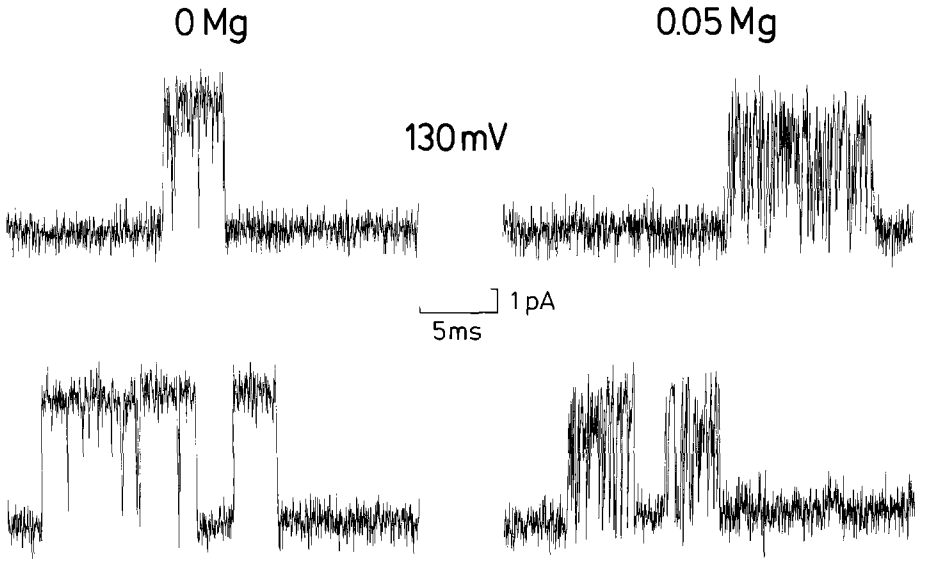

Fig. 4. Flickery block at high voltage and low $[Mg]_i$ for mutant cZ-2. The single-channel current traces were measured on different inside-out patches at 130 mV in 0 (left) and 0.05 m*M* (right) $[Mg]_i$. Solutions (apart from $MgCl_2$) are as in Fig. 2. The currents were sampled at 50 kHz and filtered with an 8-pole-Bessel filter at 10 kHz

Conditions using high $[Na]_i$ were chosen in order to increase the magnitude of the single-channel currents. In Fig. 2, single-channel current traces recorded from inside-out patches are shown at different voltages and $[Mg]_i$. It can be seen that the single-channel current amplitudes are reduced at non-zero $[Mg]_i$, especially at high voltages. The channel events display a complex gating behavior which seems to be independent of voltage. Quite often long openings (> 5 ms) without measurable interruptions can be seen (e.g. trace at 0 Mg^{2+}, 50 mV, Fig. 2). Sometimes long openings are interrupted by brief but detectable closures (e.g. trace at 0 Mg^{2+}, 70 mV, last opening, Fig. 2); in some patches the channels exhibited a very rapid bursting behavior in which no clear open-channel current level could be measured (e.g. lower left trace in Fig. 2). Even at 0 Mg^{2+} the open-channel current variance is increased as compared to the baseline variance, even if only long openings (with no resolved closings) are analyzed (see Fig. 5 and below).

In Fig. 3, single-channel current amplitudes at different $[Mg]_i$ are plotted versus voltage. The current amplitudes were exclusively determined from long openings without bursting behavior (Fig. 2, trace at 50 mV and 0 Mg^{2+}). At 0 Mg^{2+}, the current-voltage relationship is basically linear with a slope of 38.0 ± 1.1 pS. This value is higher than that obtained by Stühmer et al. (1989) from inward curents; they report a value of 13 pS for a similar mutant (cZ-1). The smaller value can be explained by their use of 1.8 m*M* Ca^{2+} in the recording pipette, a concentration which reduces inward single-channel currents significantly (see companion paper, Pusch (1990)).

The voltage-dependent reduction of the single-channel currents even at quite low Mg^{2+} concentrations (0.1 m*M*) makes it clear that $[Mg]_i$ exerts its blocking effect mainly be reducing the single-channel current amplitude. One cannot exclude the possibility that Mg^{2+} also affects the gating properties of the channel; however, the qualitative behavior suggests that this is not the case.

Taking into account the concentration- as well as the voltage-dependence of Mg^{2+} block, the I-V's were analysed according to the following equation.

$$I = P \frac{VF^2}{RT} \frac{1-\exp\left(-\frac{F(V-V_r)}{RT}\right)}{1-\exp\left(-\frac{FV}{RT}\right)} \frac{1}{1+\frac{[Mg]}{K_d(0)}\exp\left(\frac{\delta z FV}{RT}\right)}. \quad (1)$$

The first part of the equation represents the Goldman-Hodgkin-Katz equation (GHK equation) (Goldman 1943; Hodgkin and Katz 1949) which serves as a description of the I-V's in the absence of Mg^{2+} and is characterized by the permeability P and the reversal potential V_r which both depend on the ionic conditions on the intra- and extracellular side. For the I-V's shown in Fig. 3 the ionic conditions were approximately symmetrical (see legend of Fig. 3) such that $V_r \approx 0$ mV. The second term describes a simple voltage-dependent block (Woodhull 1973) and is characterized by the half-maximal blocking concentration $K_d(0)$ at $V = 0$ and the electrical distance δ. $z = 2$ is the valence of the blocking particle (Mg^{2+}); the remaining symbols have their usual meaning. The smooth lines in Fig. 3 were obtained by fitting (1) to all data points shown in Fig. 3 and using the same values of P, V_r, $K_d(0)$ and δ for all points. The effect of $[Mg]_i$ can be described by a simple first-order blocking mechanism. The values obtained from the fit are:

$$K_d(0) = (1.75 \pm 0.67)\ \text{m}M\,, \quad \delta = 0.32 \pm 0.06$$

$$V_r = (-3.2 \pm 1.8)\ \text{mV}\,, \quad P = (9.28 \pm 0.21) \cdot 10^{-18}\ \text{mol s}^{-1}\,.$$

One important question concerning the mechanism of Mg^{2+} block is whether Mg^{2+} reduces the single-channel current in a graded manner or whether it produces a flickery block, i.e. the binding of Mg^{2+} to the channel causes channel closure for short, unresolvable periods. If a flickery block is not too fast, it produces an increase in the open-channel current noise. The traces in Fig. 2 do not clearly show an increase in noise at 0.5 m*M* Mg^{2+} as compared to 0 Mg^{2+}. However, at high voltages and

lower Mg^{2+} concentrations, a substantial increase in open-channel noise could be observed. This effect is illustrated in Fig. 4 in which single-channel current traces in 0 and 0.05 m*M* Mg^{2+} at 130 mV from two different patches are shown. At 0.05 m*M* Mg^{2+} a large increase in the frequency of brief, incompletely resolved closings is evident, suggesting that Mg^{2+} acts as a fast blocker, closing the channel completely for short times.

3. *Variance analysis of the open-channel noise*

The level of resolution of the data is not sufficient to investigate the spectral properties of the open-channel noise in detail. However, the variance of the single-channel current gives an indication as to the noise properties.

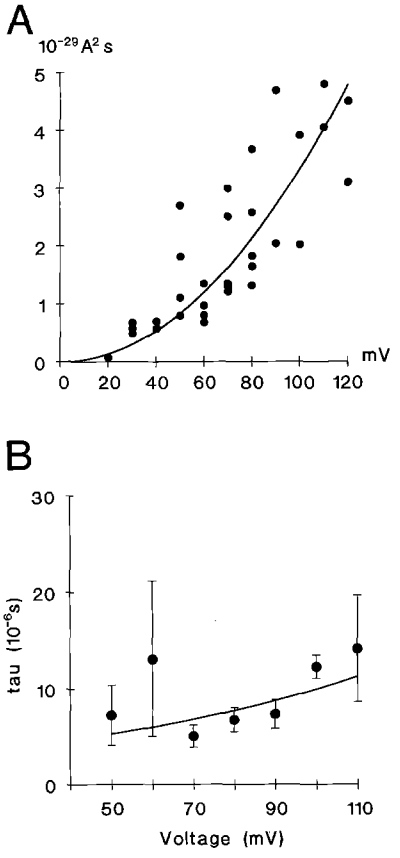

Fig. 5A, B. Open-channel noise properties of cZ-2 single-channel currents. **A** Open-channel current variance divided by the bandwidth of the recording versus test voltage. The variance was calculated as described in 'Methods'. The solid line represents a parabola of the form αV^2 with $\alpha = 3.32 \cdot 10^{-27}$ S^2 s. **B** Mean dwell time of Mg^{2+} versus voltage. For several patches at different $[Mg]_i > 0$ and voltages ≥ 50 mV variance values W were determined as described in 'Methods'. The variance was corrected for the increase in noise observed at 0 Mg^{2+} as follows: At 0 Mg^{2+} the variance W can be described by $W \approx 2.3 \cdot 10^{-6}$ s $\cdot$ i^2 $\cdot$ Bandwidth (see Fig. 5A and text). This value, calculated with mean current i, was subtracted from the variance values at $[Mg]_i > 0$. From the corrected values τ was calculated according to (5). At least two values for each voltage were averaged. The error bars are statistical standard deviations. The solid line represents the function $\tau = 2.8$ µs $\cdot \exp(0.32\, VF/(RT))$

An increase in the open-channel noise compared with the baseline noise could be observed even in the absence of $[Mg]_i$. The variance, W, divided by the bandwidth, f, in the absence of Mg^{2+} followed roughly a quadratic dependence on the single-channel current (Fig. 5A) as is expected for brief unresolved closings:

$$\frac{W}{f} \propto i^2 . \tag{2}$$

For this kind of variance analysis only relatively long openings without resolved closings to the baseline were included. The origin of this increased noise is probably due to a fast gating process or to low contaminant levels of divalent cationic blocking ions. Actually, in Fig. 5A W/f is plotted versus voltage; but, since at 0 Mg^{2+}, i is proportional to V, the quadratic dependence is preserved, and taking $\gamma = 38$ pS, the solid line in Fig. 5A corresponds to $W/f = 2.3 \cdot 10^{-6}\, s\, i^2$.

For a simple block model

$$\text{Open} \underset{k_{-1}}{\overset{[\text{Mg}]\, k_1}{\rightleftarrows}} \text{Blocked}$$

the power spectrum of the open-channel current, S, is a simple Lorentzian with cut-off frequency, $f_0 = k_{-1} + k_1$ [Mg]. Therefore, the variance, W, can be calculated as the integral of the power spectrum over the recording bandwidth f:

$$W = \int_0^f S(\varphi)\, \mathrm{d}\varphi$$

$$= \frac{2i^2\,[\text{Mg}]}{\pi K_d} \arctan\left(\frac{2\pi f}{k_{-1}} \frac{1}{1+[\text{Mg}]/K_d}\right) \tag{3}$$

with the mean current i and

$$K_d = \frac{k_{-1}}{k_1} . \tag{4}$$

To estimate the voltage-dependent rate constants k_1 and k_{-1}, (3) was solved for $\tau = 1/k_{-1}$ which represents the mean dwell time of the blocked state at voltage V, and is independent of [Mg] within the model:

$$\tau = \frac{1}{k_{-1}} = \frac{1+[\text{Mg}]/K_d}{2\pi f} \tan\left(\frac{W \pi K_d}{2\,[\text{Mg}]\, i^2}\right). \tag{5}$$

The variance W was measured for several patches at different $[Mg]_i > 0$ and different voltages ≥ 50 mV. From these values τ was calculated according to (5) assuming $K_d(V) = K_d(0) \exp(-2\delta VF/(RT))$ with the values for $K_d(0) = 1.75$ m*M* and $\delta = 0.32$ determined from the amplitude reduction by Mg^{2+} (see above). In Fig. 5B averaged values obtained in this way are plotted versus voltage. The noise observed at 0 Mg^{2+} was taken into account as described in the figure legend. It can be seen that τ ranges from 5 to 14 µs. The solid line in Fig. 5B represents an exponential function of the form

$$\tau = \tau_0 \exp\left(\frac{\delta VF}{RT}\right) \tag{6}$$

where $\delta = 0.32$ (as above) and $\tau_0 = 2.8$ µs. This kind of voltage dependence is expected for a simple voltage-dependent block model and is consistent with the data shown in Fig. 5 B. Together with the value for $K_d(0)$, this value of τ_0 yields estimates of the block and unblock rate constants of the order $k_1 = 2 \cdot 10^8\ M^{-1}\ s^{-1}$ and $k_{-1} = 3.6 \cdot 10^5\ s^{-1}$ at 0 mV. At 130 mV, which corresponds to the traces shown in Fig. 4, the mean dwell time of Mg^{2+} is, according to (6), ≈15 µs which is below the limit of clearly resolving the block as full closings.

4. A quantitative analysis of the Mg^{2+} block for wild-type II channels

Type II channels were used for a quantitative analysis because they show a high level of expression in oocytes and to enable mutant channels to be compared with the wild-type concerning open-channel Mg^{2+} block.

Instantaneous current-voltage relationships (I-V's) at different intracellular Mg^{2+} concentrations were constructed from raw tail currents as described in *Methods*. Figure 6 shows representative I-V's for type II channels at different intracellular Mg^{2+} and Na^+ concentrations. The Mg^{2+} blocking is evidently more pronounced at higher $[Na]_i$.

The I-V's were analysed according to (1), which describes a simple voltage-dependent block mechanism. The parameters describing the block [$K_d(0)$ and δ] were determined in the following way:

For a given $K_d(0)$ and δ the values for P and V_r were determined for each I-V individually using linear regression, so that the mean square deviation of the I-V and (1) would be minimal. The optimal values for $K_d(0)$ and δ were then fixed iteratively in order to minimize the total mean square deviation of all I-V's. For this the mean square deviations of each I-V were weighted with the inverse square of the maximum current-point of the corresponding I-V. In order to exclude the possible effect of extracellular Ca^{2+} ions, only currents for $V \geq -30$ mV at 125 m*M* $[Na]_i$ and $V \geq -10$ mV at 30 m*M* $[Na]_i$ have been included in the fit. At these voltages the blocking effect by extracellular Ca^{2+} ions is negligible. Because the block seems to vary at different intracellular Na^+ concentrations, the fitting procedure was applied for the determination of $K_d(0)$ and δ at fixed $[Na]_i$.

The solid lines shown in Fig. 6 were obtained by the procedure described above; the corresponding values for $K_d(0)$ and δ are listed in Table 1. It can be seen that all I-V's are well-described by (1). The electrical distance δ of 0.25 at 30 m*M* $[Na]_i$ corresponds to an e-fold increase in blocking per 50 mV. This value is virtually the same as the value of 49 mV reported by Pusch et al. (1989). However, the half-maximal blocking concentration of Mg^{2+} at $V = 0$ for type II channels in 30 m*M* $[Na]_i$ is higher than the value of 3–5 m*M* estimated by Pusch et al. (1989). Considering the block parameters at different $[Na]_i$ it is clear that the apparent affinity for Mg^{2+} increases with increasing $[Na]_i$. This effect will be discussed below.

The values in Table 1 were obtained assuming a simple blocking mechanism. Pusch et al. (1989) observed

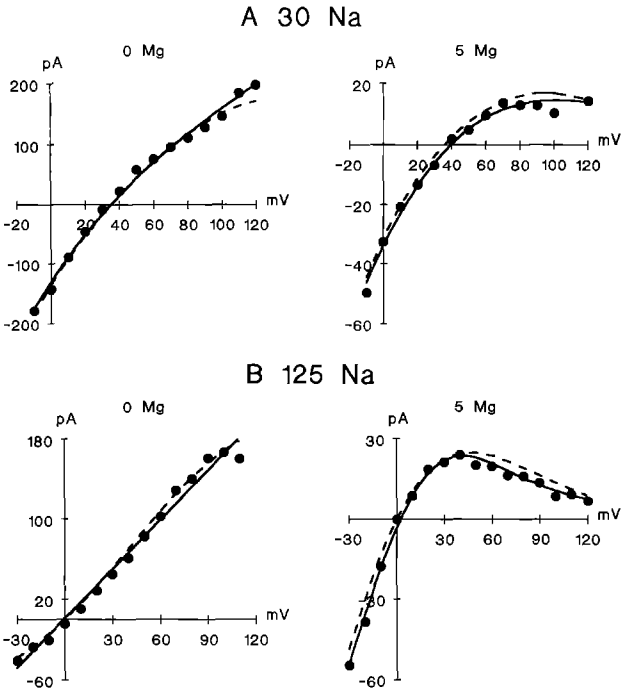

Fig. 6 A, B. Instantaneous current-voltage relationships for wild-type II. The I-V's were derived from the tail currents as described in 'Methods'. The pipette solution was in all cases normal frog Ringer (see 'Methods'), the bath solution in **A** (in m*M*): 30 NaCl, 90 KCl, 10 KOH-HEPES, 10 KOH-EGTA, pH 7.2; in **B**: 105 NaCl, 10 NaOH-HEPES, 10 NaOH-EGTA, 2.5 KCl, pH 7.2. $[Mg]_i$ is given in m*M*. The solid lines represent fits of (1) with the parameters given in Table 1. The dashed lines were obtained with the '3B2S' model described in the discussion

Table 1. Mg^{2+}-block parameters for wild-type II. Parameters describing the Mg^{2+} block obtained by a fit of (1) to several I-V's for wild-type II channels. $K_d(0)$ denotes the apparent half-maximal block concentration of Mg^{2+} at $V = 0$ and δ the apparent electrical distance (see (1)). The error estimations for $K_d(0)$ and δ were obtained as described in 'Methods'

$[Na]_{int}$ in m*M*	$K_d(0)$ in m*M*	δ	Number of I-V's
10	46	0.29	5
30	21.5±4.7	0.25±0.02	37
≈125	13.0±2.2	0.50±0.02	8

a supralinear dependence on Mg^{2+} of a parameter which is equivalent to $c/K_d(0)$ for a simple block mechanism. Therefore they suggested that such a simple blocking mechanism may not accurately describe block by Mg^{2+}. One method of describing more complicated mechanisms is to introduce a variable Hill coefficient n:

$$I = P \frac{VF^2}{RT} \frac{1-\exp\left(-\frac{F(V-V_r)}{RT}\right)}{1-\exp\left(-\frac{FV}{RT}\right)} \cdot \frac{1}{1+\left(\frac{c}{K_d(0)}\right)^n \exp\left(\frac{\delta z F V}{RT}\right)}. \quad (7)$$

However, a fit of the type II I-V's at 30 mM $[Na]_i$ with the Hill-coefficient n as an additional free parameter did not yield a significant improvement in fit and the values obtained for $K_d(0)$ and δ are similar to those in Table 1 (i.e., $K_d(0) = 20.4$ mM, $\delta = 0.25$). The Hill coefficient obtained has a value of $n = 1.04$, not significantly different from 1. The nonlinearity observed by Pusch et al. (1989) could be attributed to the fact that they included block by external agents in their analysis, which, owing to the larger number of free parameters, introduced larger scatter in the parameters describing the Mg^{2+} block.

Discussion

A multi-ion pore model describing the Mg^{2+} block

The apparent concentration for half-maximal block by Mg^{2+}, $K_d(0)$, obtained from the macroscopic tail currents, decreases with increasing $[Na]_i$ as Na^+ is replaced with K^+ (see Table 1). This effect would not be expected unless there were some interaction between Mg^{2+} and other ions in the solution. Given the composition of the solutions, the best candidates for such an interaction are Na^+ and K^+ because the Na^+ channel is impermeable to negative ions and the concentration of Cl^- was constant during the experiments. A theory which only assumes competition between Mg^{2+} and Na^+ for a common binding site would predict an increase of $K_d(0)$ with increasing $[Na]_i$. Thus it seems likely that both Na^+ and K^+ influence the apparent sensitivity to Mg^{2+}. In order to account for interaction between several ions, the multi-ion, three-barrier, two-site model (3B2S-model) of Begenisich and Cahalan (1980a, b) was examined to see if it could describe the data. In this model, ion permeation is described as "jumps" of the permeating ions from well to well with rates decreasing as the heights of the barriers increase. Mg^{2+} would then act as a blocking particle if the energy of the inner binding site were very low and if Mg^{2+} were impermeable due to a high middle barrier for Mg^{2+}.

Allowing for multi-ion occupancy and including Na^+, K^+ and Mg^{2+} as 'permeating' species, the 3B2S-model parameters were fitted using as data points all tail current-voltage relationships for type II. The tail currents then could be described with one set of parameters (listed in Table 2) at all Na^+, K^+ and Mg^{2+} concentrations used. The dashed lines in Fig. 6 are based on the 3B2S model. It can be seen that the Mg^{2+} block is reproduced at both Na^+ concentrations. Thus the apparent increase in the Mg^{2+} affinity with increasing $[Na]_i$ and simultaneously decreasing $[K]_i$ can be explained by the model. However, it cannot be ruled out that similar models or different sets of parameters could account for the $[Na]_i$ dependence of the Mg^{2+} block equally well. The low value for the energy of the intracellular binding site for Mg^{2+} ($-6RT$) indicates the relatively high affinity for Mg^{2+} ions, whereas the high middle barrier for Mg^{2+} means that Mg^{2+} is practically impermeable. The increase in the affinity for Mg^{2+} with increasing $[Na]_i$ (and decreasing $[K]_i$) can be understood in terms of the model

Table 2. Parameters of the 3B2S-model. Barrier and binding-site energies of the 3B2S model obtained by a fit to all measured tail-current voltage relationships from type II channels. The values of the energies are in units of RT. The model corresponds to that explained in detail by Begenisich and Cahalan (1980a, b) with three ion species. w_1 represents the binding site which is located near the cytoplasmic face of the membrane, and the other barriers and wells are numerated accordingly. w_i denote binding sites, b_i denote barriers. The electrical distances d_i are assumed to be equal for all ions and the barriers are assumed to be symmetrically shaped. The single-filing restriction was applied but simultaneous occupancy of both binding sites was allowed

Ion	w_1	w_2	b_1	b_2	b_3
Na^+	0.99	−0.81	3.1	3.2	7.0
K^+	−4.2	−0.34	8.4	10.5	12.5
Mg^{2+}	−6.0	−0.55	4.5	36	1.5
		d_1	d_2		
		0.36	0.69		

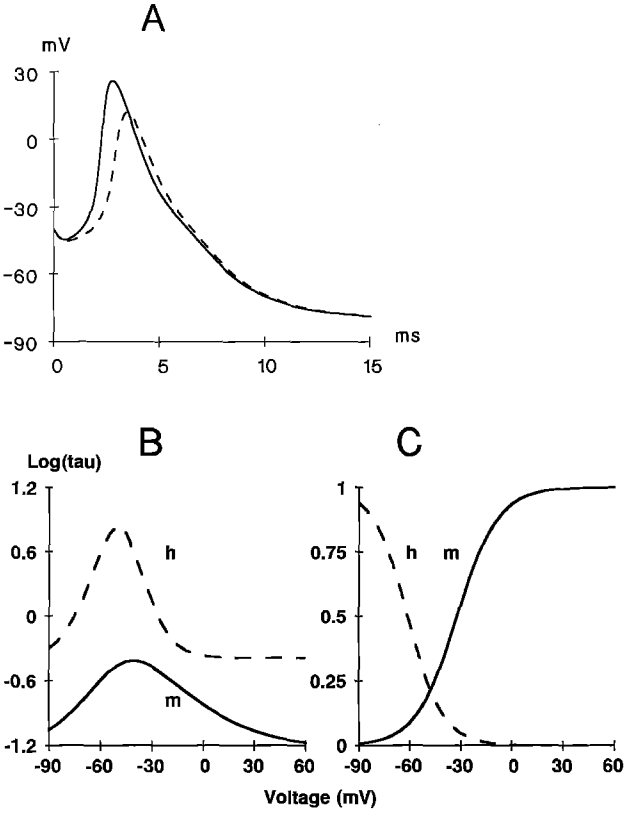

Fig. 7 A, B. Numerical calculation of action potentials at different Mg^{2+} concentrations. **A** shows action potentials at 0 (solid line) and 5 mM (dashed line) Mg^{2+}. The calculation was based on (8) and (9) and was done using the algorithm of Shampine and Gordon (1975). The voltage was first allowed to equilibrate at the resting potential (≈ -80 mV). Action potentials were then 'elicited' by a voltage step to -40 mV. The voltage-dependent parameters describing Na^+ channel open probability are illustrated in **B** and **C**. In **B** the decadic logarithms of the time constants τ_m (solid line) and τ_h (dashed line) are plotted versus voltage. In **C** the equilibrium values m_∞ (solid line) and h_∞ (dashed line) are shown. The values for τ_m, τ_h, m_∞ and h_∞ were chosen to be similar to those of the type II Na^+ channel. The other parameters were $C_m = 5$ pF, $E_{Na} = 50$ mV, $g_{Na} = 100$ nS, $E_{Leak} = -80$ mV, $g_{Leak} = 2$ nS, $K_d(0) = 15$ mM and $\delta = 0.25$

as a decreased competition between K^+ and Mg^{2+} at low internal K^+, which then increases the probability that Mg^{2+} will block the channel.

The mechanism of the Mg^{2+} block

Intracellular Mg^{2+} blocks Na^+ outward currents in all four cloned Na^+ channel types studied (Fig. 1). In addition, endogenous Na^+ channels in chromaffin cells are blocked by $[Mg]_i$. Mg^{2+} block could explain the decrease in maximum conductance at high voltages which has been observed in several preparations (Pappone 1980; Almers et al. 1984; Stühmer et al. 1987). Fahlke and Ruppersberg (1988) have studied in detail the decrease of Na^+ outward currents in human skeletal muscle which occurs despite the larger driving force for Na^+ ions. They attributed their results to a conformational change of the Na^+ channel at high voltages. Their intracellular solution, however, contained 1.5 m*M* Mg^{2+}. This makes it likely that the decrease of the currents is due to voltage-dependent block by Mg^{2+}.

Direct evidence regarding the blocking mechanism is provided by single-channel measurements in the mutant cZ-2. First, these measurements showed that the main effect of Mg^{2+} results in a voltage-dependent reduction of the single-channel amplitude. Furthermore, noise analysis of the open-channel current showed that it is not decreased in a gradual manner, but that Mg^{2+} most likely induces a fast, flickery block with closings that cannot be resolved in a patch-clamp experiment, but which significantly increase open-channel noise.

A blocking effect of internal mono- and divalent guanidinium analogues with similar voltage and $[Na]_i$ dependence as the Mg^{2+} block has been described by Danko et al. (1986). It seems likely that these agents act at the same site as Mg^{2+}.

The physiological significance of the Mg^{2+} block

Reports of free $[Mg]_i$ vary between 0.4 and 3.7 m*M* for muscular tissue (Blatter and McGuigan 1988). Changes in free $[Mg]_i$ due to ATP hydrolysis may reach the millimolar range during excess energy consumption. In order to examine the effect on action-potential firing when Na^+ channels are blocked by Mg^{2+}, a simple Hodgkin-Huxley model (Hodgkin and Huxley 1952) which includes a Na^+ ion and a leakage conductance was solved numerically at 0 and 5 m*M* Mg^{2+}. The underlying differential equations describing activation and inactivation of the Na^+ conductance and the membrane voltage V are given by

$$\frac{dm}{dt}(t) = \frac{m_\infty(V) - m(t)}{\tau_m(V)}$$
$$\frac{dh}{dt}(t) = \frac{h_\infty(V) - h(t)}{\tau_h(V)} \qquad (8)$$
$$\frac{dV}{dt}(t) = \frac{-I}{C_m}.$$

C_m is the membrane capacitance, and $I = I_{Na} + I_{Leak}$, the total ionic current. The leak current is given by $I_{Leak} = g_{Leak}(V - E_{Leak})$ and for simplicity the leak conductance g_{Leak} is considered not to be voltage-dependent. The Na^+ current is, according to the Hodgkin-Huxley model, proportional to $m^3 h$ and is affected by intracellular Mg^{2+} in the following way:

$$I_{Na} = m^3 h g_{Na}(V - E_{Na}) \cdot \frac{1}{1 + \frac{[Mg]}{K_d(0)} \exp\left(\frac{2\delta VF}{RT}\right)}. \qquad (9)$$

Figure 7A shows the calculation of action potentials at 0 Mg^{2+} (solid line) and 5 m*M* Mg^{2+} (dashed line). $K_d(0)$ was assumed to be 15 m*M* and $\delta = 0.25$. At 5 m*M* Mg^{2+} a reduction in the amplitude of the action potential by 15 mV and a delay of the maximum amplitude by 0.6 ms can be observed. Thus an increase of intracellular free Mg^{2+} by large rates of ATP hydrolysis, apart from known effects on other channel types, might significantly alter excitability properties of a cell simply because of voltage-dependent block of Na^+ channels.

Mg^{2+} block is a common feature of ion channels

Inhibitory effects of internal Mg^{2+} have been demonstrated for a variety of ion channels. The Mg^{2+} block described by Horie et al. (1987) for ATP-sensitive K^+ channels in guinea-pig ventricular cells is similar to the block of Na^+ channels described here. However, the block and unblock rate constants are one order of magnitude smaller in the ATP-sensitive K^+ channels as compared to the Na^+ channel mutant cZ-2. Other K^+ channels blocked by intracellular Mg^{2+} at low concentrations are inwardly rectifying K^+ channels (Matsuda et al. 1987; Ishihara et al. 1989) and muscarinic K^+ channels (Horie and Irisawa 1987). Thus intracellular Mg^{2+} seems to have direct regulatory effects on membrane permeability. Also the functionally important outward rectification of N-methyl-D-aspartate sensitive channels results largely from a voltage-dependent open-channel block by external Mg^{2+} (Nowak et al. 1984; Mayer et al. 1984).

A physiological significance of the Mg^{2+} block is suggested by the effect of Mg^{2+} on simulated action potentials. However, measurements of action potentials in nerve and muscle cells are required to resolve this question definitely. From a biophysical viewpoint, Mg^{2+} block offers a tool for the investigation of structure-function relationships of cloned Na^+ channels expressed in oocytes which is exploited in the companion paper (Pusch 1990).

References

Almers W, Roberts WM, Ruff RL (1984) Voltage clamp of rat and human skeletal muscle: measurements with an improved loose-patch technique. J Physiol (London) 347:751–768

Begenisich TB, Cahalan MD (1980a) Sodium channel permeation in squid axons I: reversal potential measurements. J Physiol (London) 307:217–242

Begenisich TB, Cahalan MD (1980b) Sodium channel permeation in squid axons II: non-independence and current-voltage relations. J Physiol (London) 307:243–257

Bezanilla F, Armstrong M (1977) Inactivation of the sodium channel. J Gen Physiol 70:549–566

Blatter LA, McGuigan AS (1988) Estimation of the upper limit of the free magnesium concentration measured with Mg-sensitive microelectrodes in ferret ventricular muscle: *(1)* Use of the Nicolsky-Eisenman equation and *(2)* in calibrating solutions of the appropriate concentration. Magnesium 7:154–165

Caceci MS, Cacheris WP (1984) Fitting curves to data. Byte 9:340–362

Danko M, Smith-Maxwell C, McKinney L, Begenisich T (1986) Block of sodium channels by internal mono- and divalent guanidinium analogues. Biophys J 49:509–519

Fahlke C, Ruppersberg JP (1988) Saturation effects and rectifier properties of sodium channels in human skeletal muscle. Eur Biophys J 16:307–312

Fenwick EM, Marty A, Neher E (1982) Sodium and calcium channels in bovine chromaffin cells. J Physiol (London) 331:599–635

Goldman DE (1943) Potential, impedance, and rectification in membranes. J Gen Physiol 27:37–60

Hamill OP, Marty A, Neher E, Sakmann B, Sigworth FJ (1981) Improved patch-clamp techniques for high-resolution current recording from cells and cell-free membrane patches. Pflügers Arch 391:85–100

Hodgkin AL, Huxley AF (1952) A quantitative description of membrane current and its application to conduction and excitation in nerve. J Physiol (London) 117:500–544

Hodgkin AL, Katz B (1949) The effect of sodium ions on the electrical activity of the giant axon of the squid. J Physiol (London) 108:37–77

Horie M, Irisawa H (1987) Rectification of muscarinic K^+ current by magnesium ion in guinea pig atrial cells. Am J Physiol 253:H210–H214

Horie M, Irisawa H, Noma A (1987) Voltage-dependent magnesium block of adenosine-triphosphate-sensitive potassium channel in guinea-pig ventricular cells. J Physiol (London) 1987:251–272

Ishihara K, Mitsuiye T, Noma A, Takano M (1989) The Mg^{2+} block and intrinsic gating underlying inward rectification of the K^+ current in guinea-pig cardiac myoocytes. J Physiol (London) 419:297–320

Kayano T, Noda M, Flockerzi V, Takahashi H, Numa S (1988) Primary structure of rat brain sodium channel III deduced from the cDNA sequence. FEBS Lett 228:187–194

Marty A, Neher E (1983) Tight-seal whole-cell recording. In: Sakmann B, Neher E (eds) Single channel recording. Plenum Press, New York London, pp 107–122

Matsuda H, Saigusa A, Irisawa H (1987) Ohmic conductance through the inwardly rectifying K channel and blocking by internal Mg^{2+}. Nature (London) 325:156–159

Mayer ML, Westbrook GL, Guthrie PB (1984) Voltage-dependent block by Mg^{2+} of NMDA responses in spinal cord neurones. Nature (London) 309:261–263

Methfessel C, Witzemann V, Takahashi T, Mishina M, Numa S, Sakmann B (1986) Patch clamp measurements on *Xenopus* laevis oocytes: currents through endogenous channels and implanted acetylcholine receptor and sodium channels. Pflügers Arch 407:577–588

Noda M, Ikeda T, Kayano T, Suzuki H, Takeshima H, Kurasaki M, Takahashi H, Numa S (1986) Existence of distinct sodium channel messenger RNAs in rat brain. Nature (London) 320:188–192

Nowak L, Bregestovski P, Ascher P, Herbert A, Prochiantz A (1984) Magnesium gates glutamate-activated channels in mouse central neurones. Nature (London) 307:462–465

Pappone PA (1980) Voltage-clamp experiments in normal and denervated mammalian skeletal muscle fibres. J Physiol (London) 306:377–410

Pusch M (1990) Divalent cations as probes for structure-function relationships of cloned voltage-dependent sodium channels. Eur Biophys J 18:327–333

Pusch M, Conti F, Stühmer W (1989) Intracellular magnesium blocks sodium outward currents in a voltage- and dose-dependent manner. Biophys J 55:1267–1271

Shampine LF, Gordon MK (1975) Computer solutions of ordinary differential equations: the initial value problem. Freeman, San Francisco

Stühmer W, Methfessel C, Sakmann B, Noda M, Numa S (1987) Patch clamp characterization of sodium channels expressed from rat brain cDNA. Eur Biophys J 14:131–138

Stühmer W, Conti F, Suzuki H, Wang X, Noda M, Yahagi N, Kubo H, Numa S (1989) Structural parts involved in activation and inactivation of the sodium channel. Nature (London) 339:597–603

Woodhull AM (1973) Ionic blockage of sodium channels in nerve. J Gen Physiol 61:687–708